RSC Advances

ROYAL SOCIETY OF CHEMISTRY

www.rsc.org/advances

Designing a novel nanocomposite for bone tissue engineering using electrospun conductive PBAT/polypyrrole as scaffold to direct nanohydroxyapatite electrodeposition

Juçara G. de Castro,[ǂ] Bruno V. M. Rodrigues,[ǂ] Ritchelli Ricci, Maíra M. Costa, André F. C. Ribeiro, Fernanda R. Marciano and Anderson O. Lobo*

[1] Laboratory of Biomedical Nanotechnology (NANOBIO), Institute of Research and Development (IP&D II), University of Vale do Paraiba (UNIVAP), Sao Jose dos Campos, 12244-000, Sao Paulo, Brazil

ǂ These authors contributed equally to this work

*e-mail: aolobo@pq.cnpq.br and lobo.aol@gmail.com.

Abstract: Electrospinning is a well-recognized technique for producing nanostructured fibers capable to support cell adhesion and further proliferation. Here, we prepared a novel electrospun blend from poly (butylene adipate-co-terephthalate) (PBAT), a non-conductive and biodegradable polymer, and a conductive polymer, namely polypyrrole (PPy). Therefore, the goal was to create electrically conductive nanoscaffolds for tissue engineering applications. Furthermore, to improve the scaffold biomimetic features for bone regeneration purposes, we demonstrated the feasibility of electrodepositing nanohydroxyapatite (nHAp) onto the new hybrid scaffold. Electrochemical measurements confirmed the electrical conductivity of the novel PBAT/PPy scaffold, which allowed for the nHAp electrodeposition, further confirmed via ATR-FTIR analysis and FE-SEM micrographs. The PPy loading did not change the fibers' average diameter, although the increase in the solution conductivity was probably responsible to lead to electrospun mats with smaller beads and lower presence of flattened regions

compared to PBAT neat. The hybrid scaffold was more hydrophilic than PBAT neat. The first presented an advanced contact angle (ACA) of 84º, whilst the latter presented an ACA of 115º. The incorporation of PPy to PBAT maintained the ability of the generated scaffold to support cell adhesion with no changes in MG-63 cell viability. However, PBAT/PPy scaffold presented higher values of alkaline phosphatase, an important indicator of osteoblasts differentiation. In conclusion, we demonstrated a feasible approach to create electrically conductive nanoscaffolds, which are capable to undergo to nHAp electrodeposition in order to generate materials that are more hydrophilic and with improved cell differentiation. These results show the potential of application of this novel scaffold towards bone regenerative medicine.

Keywords Poly (butylene adipate-co-terephthalate); polypyrrole; electrospinning; electrodeposition; nanohydroxyapatite; cytotoxicity; ALP

1. Introduction

In the recent decades, many processing techniques have been employed for producing nanoscaffolds aiming at tissue engineering applications. [1, 2] In the field of bone tissue regeneration, it is essential to reach bone-extracellular matrix (ECM)-architectures like, which in turn play a crucial role in controlling cell adhesion and further differentiation. Among the aforementioned processing techniques, electrospinning occupies a prominent place due to its recognized ability to produce tridimensional fibrous structures, which is mandatory for applications in the field of bone tissue engineering.[3, 4]

Electrospun nanofibers scaffolds present a wide range of potential applications, owing to their high porosity, pore interconnectivity and physical-chemical properties. We can address applications in the fields of wound dressing, [5] membranes, [6] tissue engineering [3] or even as carriers for drug delivery. [7] Combining all the above mentioned properties with the ability of electrospun polymeric scaffolds to support cell adhesion and further differentiation and proliferation, electrospinning has been used as primary technique to produce fibrous nanoscaffolds for many tissue engineering applications. [3]

Polyesters, from synthetic or natural sources, have been widely studied towards their potential for biomedical applications, more specifically in tissue engineering applications. [8-10] Recently, poly (butylene adipate-co-terephthalate) (PBAT), a copolymer, aroused as a promising alternative. [11-17] This polymer is very flexible and has a wide range of interesting properties, such as high elongation at break and biodegradability. [18]

Ribeiro Neto et al. [19] prepared nanocomposites based on PBAT and hydroxyapatite (HA) particles via electrospinning and spin coating. In this study, Ribeiro Neto et al.[19] verified not only that these novel nanocomposites ensured the attachment, proliferation and differentiation of adipose stem cells, but also that implants using these materials triggered only a mild inflammatory response. Recently, our group has demonstrated the preparation of electrospun PBAT/superhydrophilic multi-walled carbon nanotubes with enhanced mechanical properties and adequate cell viability levels. [20] Nevertheless, to date materials from the electrospinning of PBAT and their blends have received little attention related to their preparation and application. [11, 19, 21, 22]

Conductive polymers have been often applied to produce scaffolds for tissue engineering applications. [23-28] Furthermore, it has been also hypothesized a mechanism

in which the piezoelectric signals can regulate the bone growth. [29] At the cellular level, the bone cell type that plays an important role in the bone structure development and appears to be involved in bone mechanotransduction, the osteocytes, was identified.[30] Consequently, for bone regeneration, these cells communicate with other bone cells, such as osteoblasts and osteoclasts. Therefore, the influence of electrical stimulation on bone healing has been studied *in vitro* and *in vivo.* [31-34]

Electrodeposited nanohydroxyapatite (nHAp) presents a great similarity to the mineral component of natural bone, as regards of dimensions and microstructure, whilst it shows excellent bioactivity, biocompatibility and osteoconductivity. [35-37] Owing to these outstanding properties, nHAp has been long evaluated for applications in the field of bone tissue/regeneration. [37-40] Previous study of our group has demonstrated an effective, fast and low-cost way to electrodeposit nHAp layers onto modified vertically aligned multi-walled carbon nanotubes (VAMWCNTs). [41] To date, the electrodeposition of nHAp onto polyesters polymeric fibers, such as electrospun fibers, has been underexplored since the lack of conductivity of these scaffolds.

Polypirrole (PPy), a well-known conductive polymer, has been often applied as a biomaterial due to the possibility of generating cellular stimulus, adhesion and proliferation besides of bacteria reduction. [42-45] To date several authors electrospun polyesters/pyrrole nano/microfibers for tissue engineering. [25, 46-49] However, so far there is no study published using PBAT/PPy blends towards tissue engineering applications. Moreover, there is no study addressing the electrodeposition of nHAp on polyesters surfaces, as previously mentioned, due to the lack of conductivity of these polymers. Herein, we presented for the first time the preparation of electrospun PBAT/PPy fibers aiming at tissue engineering applications. In this context, we evaluated the cytotoxicity and alkaline phosphatase activity (ALP) using human osteoblasts. This novel

biomaterial presented promising properties for future *in vivo* applications aiming at bone tissue engineering.

2. Experimental

2.1 Materials

BASF SE kindly provided the pellets of PBAT (commercial Ecoflex® F Blend C1200). The solvents used in this investigation were dimethylformamide (DMF, Sigma-Aldrich, ≥ 99%) and chloroform (Sigma-Aldrich, ≥ 99%). Calcium nitrate tetrahydrate [$Ca(NO_3)_2 \cdot 4H_2O$] and ammonium phosphate dibasic [$(NH_4)_2HPO_4$] were also purchased from Sigma-Aldrich, with high chemical grade. Any mention of other chemicals has the respective origin indicated along the text.

2.1.Electrospinning of PBAT/PPy fibers

Electrospinning was carried out from solutions containing PBAT and PPy at 12 wt% and 1 wt%, respectively, using chloroform and DMF as solvent system (60/40). In a typical preparation, PBAT was dissolved in chloroform during 2 h, under vigorous stirring, while PPy was dispersed in DMF under sonication (VCX 500 – Sonics) during 60 min. After PPy was fully dispersed, the two solutions were mixed and the resulting solution was stirred during 20 h until complete homogenization. Electrospinning optimal conditions were established as follows: 13 kV, 10 cm as needle-collector distance, solution flow rate of 1 mL h^{-1}. The counter electrode was covered with aluminum foil to collect the electrospun mats, which were easily displaced to proceed

with the characterizations and biological assays. During electrospinning, we carefully controlled the temperature (21-23 ºC) and humidity (45-55%).

2.2. Electrodeposition of nHAp onto PBAT/PPy fibers

First, we evaluated the electrochemical performance of the PBAT/PPy scaffolds by collecting cyclic voltammograms using a classical electrode cell with a well-known potassium ferrocyanide (II) (5 mM, Synth-F1008) in 0.1 M KCl $_{(aq.)}$ solution. After that, we electrodeposited nHAp crystals on PBAT/PPy scaffolds using a standard three-electrode cell controlled by Autolab PGSTAT 128N. The PBAT/PPy scaffolds were employed as a working electrode by inserting it inside a copper/Teflon electrochemical cell, which exposed a fixed electrode area (~ 0.27 cm^2) to the solution, and also established electrical contact to a copper rod on the back-side. A platinum mesh was used as counter electrode, while Ag/AgCl (3 M KCl $_{(aq.)}$) as reference electrode. The electrolyte solution used was composed of 0.042 mol L^{-1} of $Ca(NO_3)_2{\cdot}4H_2O$ + 0.025 mol L^{-1} of $(NH_4)_2HPO_4$. The pH was adjusted to 4.7 and automatically measured throughout the process of electrodeposition using a pX1000 real-time pH meter (no data shown, Metrohm). Magnetic stirring and a thermostatic bath were used to maintain the process at constant stirring and temperature (~70°C), respectively. The nHAp crystals were produced on PBAT/PPy scaffolds by applying a constant potential of –3.8 V for 30 min. This set-up was chosen to promote stoichiometric nHAp with a Ca/P ratio of ~1.67.

2.3. Characterization of PBAT/PPy/nHAp fibers

PBAT/PPy fibers

ATR-FTIR (Attenuated Total Reflectance Fourier Transform Infrared Spectroscopy) was performed using a Perkin-Elmer Spotlight 400 FTIR Imaging System. Data were collected in the range of 4000-450 cm^{-1} in absorbance mode.

FE-SEM (Field-Emission Scanning Electronic Microscopy) was carried out using a Mira3 TESCAN Microscope, operating at 20.0 kV. Prior to analysis, all samples were coated with a thin layer of gold (~10 nm) using a sputter-coat system, in order to improve image acquisition.

The dynamic contact angle between a deionized water drop and the surface of the samples was measured. A Krüss contact angle device (Model DSA 100S) equipped with a recording system was used. Briefly, a single drop of deionized water (2 μL) was deposited on the surface of the samples (fixed on Teflon substrates) by an automatized dispositive (syringe-needle system) to generate a drop with accurate volume. The measurements of the angle between the interface were taken in different times (0-2400 s). All measurements were carried out in a controlled humidified atmosphere (~ 60%).

PBAT/PPy/nHAp fibers

FE-SEM (Field-Emission Scanning Electronic Microscopy) was carried out using a Mira3 TESCAN Microscope, operating at 20.0 kV, in order to characterize the nHAp crystals morphology. Prior to analysis, all samples were coated with a thin layer of gold (~10 nm) using a sputter-coat system, in order to improve micrograph acquisition. The microscope was coupled to an OEM easyEDX detector in order to determine semi-quantitatively the content of calcium (Ca) and phosphorous (P) and also to perform a mapping of these atoms directly live in the SEM micrograph. EDX and

mapping analyses were performed at 10.0 kV. For EDX analysis the samples were not coated with gold.

X-ray diffraction (XRD, X-Pert Philips) with Cu K-α radiation generated at 40 kV and 50 mA was used to characterize the microstructure and phase content of the nHAp crystals. The results were compared to the standards for HAp powder (JCPDS 01-072-1243).

2.4. Cell culture

Human osteoblasts from MG-63 cell line (ATCC® CRL-1427™) were cultured with Dulbecco's Modified Eagle Medium (DMEM, GIBCO) supplemented with 10% of Fetal Bovine Serum (FBS, GIBCO) at 37°C.

2.5. Cellular adhesion analysis

SEM (EVO MA10, Zeiss) was used to analyze the adhesion of cells over the scaffolds. Osteoblasts cultivated for 24 h over the polymeric scaffolds were fixed with fresh prepared 4% paraphormaldehyde/2.5% glutaraldehyde (Sigma-Aldrich) solution for 10 min at room temperature. Dehydration was carried out sequentially in the dishes with acetone (Sigma-Aldrich) at concentrations of 50%, 70%, 90% and 100% for 10 min each, followed by 1:1 vol/vol acetone/HMDS (Sigma-Aldrich) solution incubation for 30 min and then 100% HMDS for 30 min. The surface of the samples was sputter-coated with a thin gold layer (~10 nm).

2.6. Cellular viability assay

The cellular viability of cultured cells was determined with the MTT colorimetric assay, adapted from the method proposed by Mosmann [50]. During incubation, the MTT was reduced by dehydrogenase enzyme from mitochondria within the viable cells, precipitating the insoluble formazan crystals. All the samples pieces (10 x 10 x 1 mm) were sterilized with ethanol (70% v/v) and rinsed with PBD. MG-63 human osteoblast cells were seeded at a concentration of 2 x 10^4 cells/well. The incubation was performed under a CO_2 (5%) atmosphere, at 37 ºC, for 1 and 7 days. Latex fragments were used as positive control of cell death at the same dimensions of the substrates. After the incubation period, the samples were removed from their respective wells. Only adhered cells were incubated with MTT solution (1 mg mL^{-1}, Sigma-Aldrich, Saint Louis, Missouri, USA) for 3 h at 37 ºC.

After removal of the MTT solution, dimethyl sulfoxide (DMSO) (Sigma-Aldrich Saint Louis, Missouri, USA) was added to each well and incubated under stirring for 15 min. After complete solubilization of the dark-blue crystal of MTT formazan, the absorbance of the content of each well was measured at 570 nm with a spectrophotometer Spectra Count (Packard). The blank reference was taken from wells with DMSO only, and its value subtracted from samples and control OD. The cell viability was expressed as percentage related to the control.

2.7. Alkaline Phosphatase assay (ALP)

Osteoblasts differentiation is dependent on the expression of alkaline phosphatase enzyme. Therefore, osteogenic stimulation by the scaffolds is directly correlated to the enhancement of ALP activity. To assess the scaffolds ability to

stimulate osteoblasts differentiation, MG-63 cells were cultured on the samples in a 24 well plate for 14 and 21 days and the ALP content analyzed. The wells were washed three times with PBS at 37 °C and incubated with 2 mL of 0.1% sodium lauryl sulfate (SLS) for 30 min. The SLS/cells solution was mixed with Lowry solution (Sigma-Aldrich) and incubated for 20 min at room temperature. Folin–Ciocalteu phenol reagent (Sigma-Aldrich) was added for 30 min at room temperature to allow color development. Absorbance was measured at 680 nm. The total protein content was calculated based on albumin standard curve and expressed as μg mL^{-1}. To determine ALP activity through the releasing of thymolphthalein monophosphate, we used an Alkaline Phosphatase Kit (Labtest Diagnóstica, Belo Horizonte, BR) in accordance with the manufacturer's recommendations. First, 50 μL of thymolphthalein monophosphate were mixed with 0.5 mL of 0.3 M diethanolamine buffer for 2 min at 37 °C. The solution was then added to 50 μL of the lysates obtained from each well. After 10 min, at 37°C, 2 mL of 0.09 M Na_2CO_3 and 0.25 M NaOH were added for color development for 30 min. Absorbance was measured at 590 nm using a UV 1203 spectrophotometer. ALP activity was correlated with total protein content and expressed as ALP μmol thymolphthalein/min/mL.

2.8. Statistics analysis

Cell culture experiments were conducted in quadruplicate and all values reported as mean ± standard deviation. The difference between groups was analyzed by ANOVA test followed by Tukey´s post-hoc ($p < 0.05$).

3. Results and Discussion

Fig. 1 shows the electrochemical response (a), pH measurement (b) and current density (c) of PBAT and PBAT/PPy scaffolds.

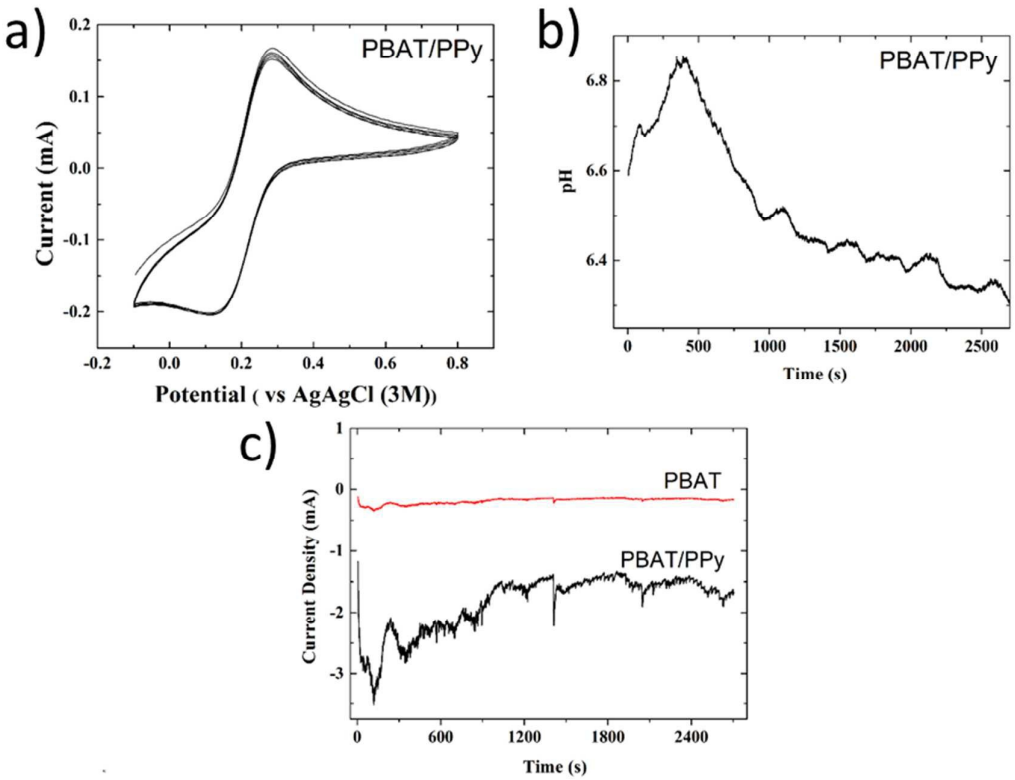

Figure 1: (a) Cyclic voltammograms of PBAT/PPy scaffolds taken at 10, 25, 50, 100 and 200 mV s^{-1} in 5 mM $K_3Fe(CN)_6$/0.1 M $KCl_{(aq.)}$. (b) pH and (c) Current density transients during electrodeposition of nHAp on PBAT/PPy scaffolds at –3.8 V vs. Ag/AgCl and T = 70 °C.

Fig. 1a shows the voltammograms recorded in 0.1 M KCl aqueous electrolyte with a sweep rate of 10-200 mV s^{-1} of the PBAT/PPy scaffolds. As depicted, the current-voltage curve of composite presented capacitive behavior between the potentials of 0.8 -0.1 V vs Ag/AgCl (3 M). The oxidation-reduction peaks at 0.28 V and 0.12 V vs. Ag/AgCl (3 M) are respectively attributed to reactions of conductive PPy polymer

incorporated to PBAT. As a direct result, PBAT/PPy scaffolds have current capacitance and current density.

Fig. 1 b shows a pH decrease for more acidic levels due to an oxidation reaction taking place at the anode ($2\ H_2O_{(l)} \rightarrow O_{2(g)} + 4\ H^+_{(aq.)} + 4e^-$), which forms H^+ during water splitting. The pH was measured between the working electrode and the counter electrode. The shape of the current transient is different, and the measured current density is much higher than those reported by Eliaz and Sridhar [51] for electrodeposition of HAp on CP-Ti at either pH = 4.2 or pH = 6.0. However, the applied potential reported by Eliaz and Sridhar [51] was –1.4 V *vs*. SCE (*i.e*. –1.356 V vs. Ag/AgCl), which resulted in less hydrogen evolution. The extensive hydrogen evolution in the present work may have been responsible for the noisy and unsteady current transient besides electrodeposition on 3D ultrathin fibers. While the kinetics of nucleation is promoted by the high overpotential, crystal growth is suppressed by the intensive H_2 evolution. As a consequence, smaller nHAp crystals are formed and the coating is governed by secondary nucleation processes.

Fig. 1 c shows a comparison between the average current density measured during nHAp electrodeposition. Clearly, we noticed that the measured current density for PBAT/PPy scaffolds was ten times higher than for PBAT. The nHAp electrodeposition process involved an evolution of hydroxyl ions on the surface electrode (PBAT/PPy scaffolds). Consequently, the hydroxyl ions, induced acid–base reaction to form HPO_4^{-2} and PO_4^{-3}, are responsible for calcium phosphate precipitation on PBAT/PPy scaffolds. [52] Diffusion process is responsible to control the electrodeposition process besides of current density and pH changing of the solution. [53] We presented all these characteristics in **Fig. 1 b and 1 c**.

Fig. 2 shows the micrographs of PBAT, PBAT/PPy and PBAT/PPy after nHAp electrodeposition.

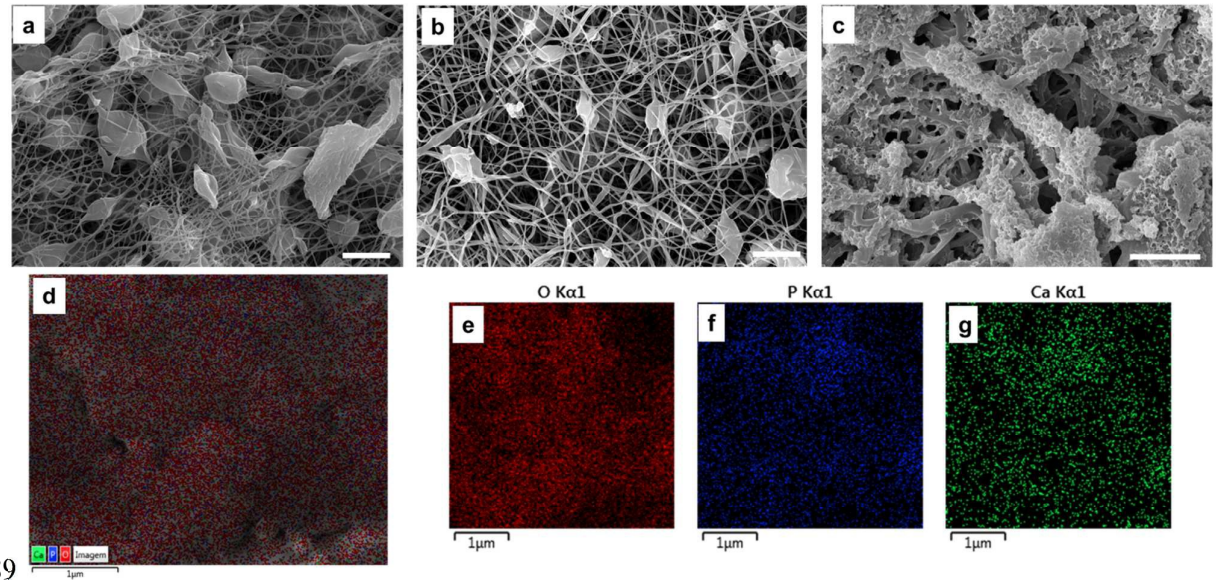

Figure 2. FE-SEM micrographs of (a) PBAT; (b) PBAT/PPy and (c) PBAT/PPy/nHAp (bar scales = 2.5 μm). EDS mapping of PBAT/PPy/nHAp in (d) layers (Ca, P, O atoms); (e) O atom; (f) P atom and (g) Ca atom.

We observed that the PPy loading did not promote significant changes in the average diameter of the fibers. PBAT presented an average diameter of 111 ± 26 nm (**Fig 2a)**, while PBAT/PPy had a small increase (132 ± 33 nm, **Fig 2b**). Both samples presented a bead-on-a-string morphology, however it can be noted that loading PPy led to smaller beads with less flattened regions. This reduction on the beads size and further fusiform aspect may be attributed to the increase in the electrical conductivity due to the presence of PPy and consequent increase in the neat charge density in the jet. [54] Electrical measurements showed that while the PBAT solution presented an electrical conductivity of 0.2 μS cm^{-2}, the introduction of PPy increased the electrical conductivity to 36.2 μS cm^{-2}. One can note that the electrodeposition onto the

PBAT/PPy scaffold surface (**Fig 2 c**) was effective and led to nHAp crystals homogeneously deposited.

Fig. 2 (d-g) shows the EDX mapping of PBAT/PPy/nHAp scaffolds. The mapping distribution of Ca, P and O atoms **(Fig 2d, f and g)** indicated a homogeneous distribution of electrodeposited nHAp onto the PBAT/PPy scaffolds. We observed a Ca/P of 1.69, which was quite close to the stoichiometric nHAp (1.67) present in bone tissue.[36]

Fig. 3 shows the XRD patterns of PBAT/PPy and PBAT/PPy/nHAp scaffolds. One can see that the apatite formation is confirmed by the presence of several characteristic XRD peaks in the diffraction patterns. The principal diffraction peaks of nHAp appear at 2-Theta values of 25.9º for reflection (002) and at 31.9º (triplet) for reflections (211), (112) (JCPDS 01-072-1243).[55]

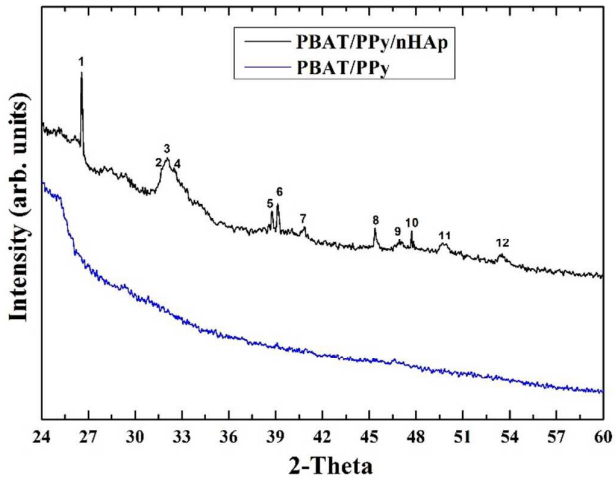

Fig. 3 shows the ATR-FTIR spectra of electrospun PBAT, PBAT/PPy and PBAT/PPy/nHAp.

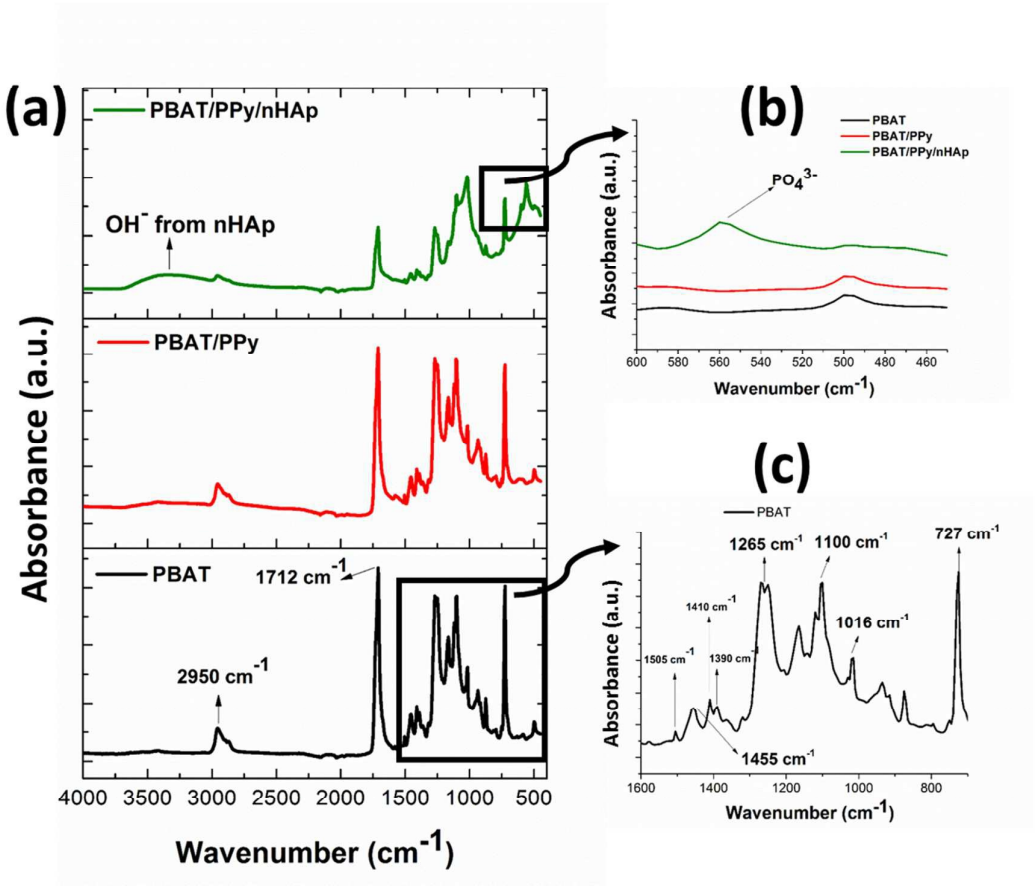

Figure 4. ATR-FTIR spectra of (a) PBAT, PBAT/PPy and PBAT/PPy/nHAp; (b) zoom in the 600-450 cm^{-1} region, showing the absorbance of the PO_4^{3-} group; (c) zoom in the 1600-700 cm^{-1} region for PBAT.

The ATR-FTIR spectra of the electrospun PBAT, PBAT/PPy and PBAT/PPy after nHAp electrodeposition (PBAT/PPy/nHAp) (**Fig. 4**) showed the characteristics peaks of the polyester (PBAT). [20] The asymmetric stretching vibration of CH_2 groups can be identified at 2950 cm^{-1}; stretching vibration of C=O at 1710 cm^{-1}; stretching of phenylene group at 1455 and 1505 cm^{-1}; trans-CH_2-plane bending vibration at 1410 and 1395 cm^{-1}; symmetric stretching vibration of C-O at 1265 cm^{-1}; C-O left-right symmetric stretching vibration absorption at 1100 cm^{-1}; bending vibration absorption of CH-plane of the phenylene ring at 1016 and 731 cm^{-1}.

The electrodeposition of nHAp on the surface of the electrospun PBAT/PPy mat could be confirmed via ATR-FTIR. The vibrational band in the region of 3500 cm^{-1} (PBAT/PPy/nHAp, **Fig. 4 a**) can be attributed to OH^- absorption peak whilst the PO_4^{3-} absorption peak could be observed at 566 cm^{-1} (**Fig 4. b**).

PBAT neat or with PPy, and nHAp are known as no cytotoxic materials, [56-59] providing a great biologic compatibility. Electrospun PBAT, PBAT/PPy and PBAT/PPy/nHAp mats presented no cytotoxic effect after the contact with cells during 1-7 days. **Fig. 5** shows the osteoblasts viability after cultivation on PBAT, PBAT/PPy and PBAT/PPy/nHAp scaffolds for 1 and 7 days.

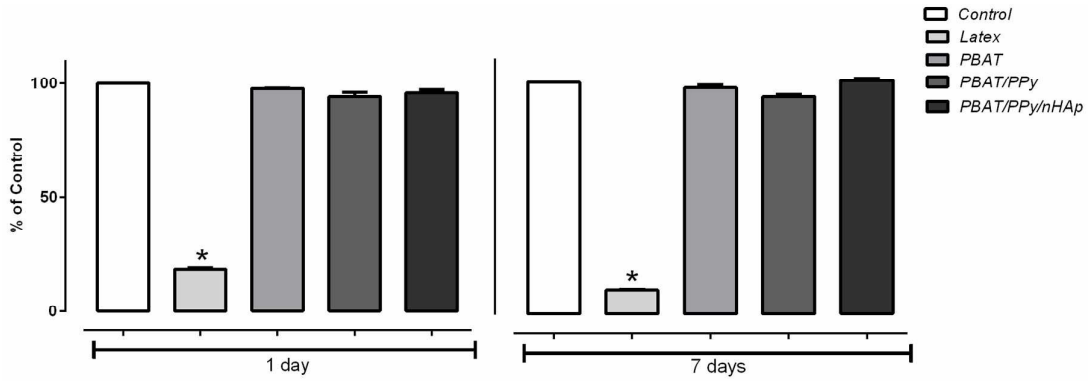

Figure 5. Cellular viability analysis of MG-63 cultured on polymeric scaffolds after 1 and 7 days. *$p < 0.05$ *vs* control.

Nevertheless, the aim of biomaterial research is not restrictive to the production of inert materials, but also to the development of scaffolds capable to improve biomaterial integration with organic tissue. The creation of a biomimetic material for bone regeneration can be mainly achieved with structure and surface manipulations [60, 61], as for example the addition of nHAp. [62, 63] Nanofiber scaffolds with tridimensional structure can enhance cellular adhesion because their arrangement is similar to extracellular matrix. [64] As **Fig. 6** shows, polymeric nanofiber mats can provide an ideal

scaffold for cells. MG-63 osteoblasts were able to adhere to the scaffolds, maintaining the classical osteoblast morphology (part of the cells was blue painted).

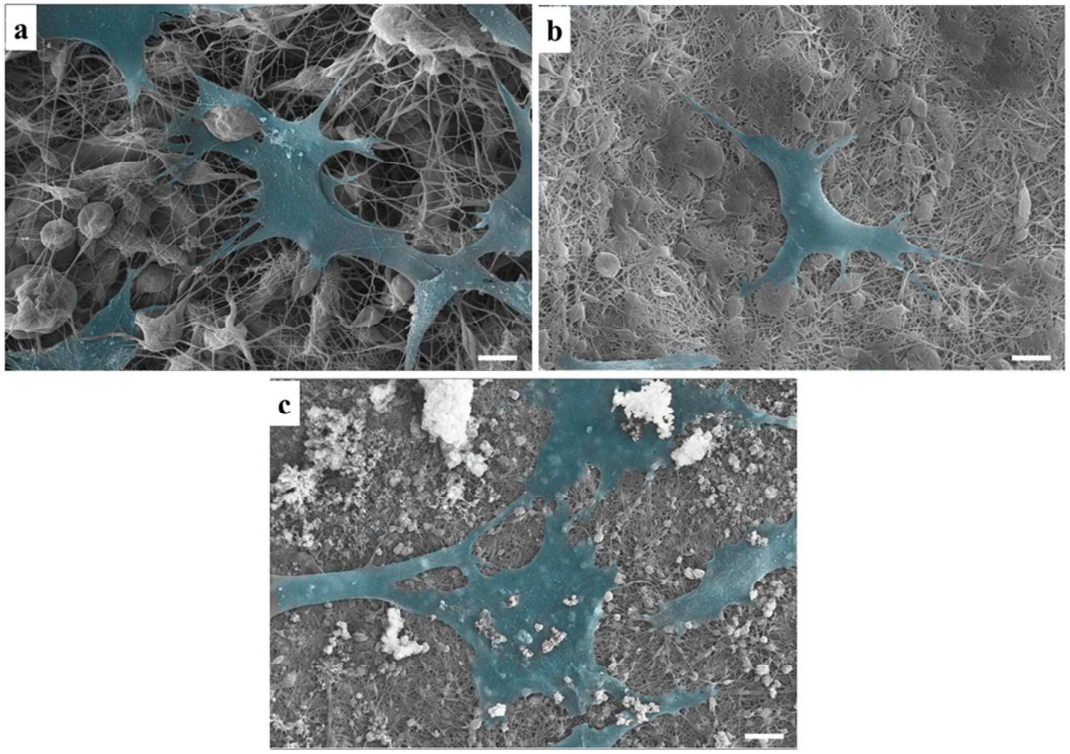

Figure 6. SEM micrographs of part of MG-63 cells (blue painted) cultured 24 h on (a) PBAT, (b) PBAT/PPy and (c) PBAT/PPy/nHap scaffolds. Scale bar = 10 μm.

Next, we evaluated the induction of osteoblasts differentiation when cultured with the polymeric scaffolds. Osteoblast differentiation is a time-dependent phenomenon that can be modulated by the cell type and stimulus. ALP increase using MG-63 culture in an osteoinductive media is expected typically after 28 days of culture.[65] **Fig. 7** shows that PPy induced an increase in ALP activity after 21 days; meanwhile the presence of nHAp was indifferent. An increase in ALP activity occurs during osteoblasts differentiation and is commonly related to calcification of bone matrix. [66] Several authors reported PPy as an enhancer of ALP activity, however the

experiments involved the use of electrical stimulation [59, 67] or osteoinductive media. [68] However, here we proved that only the PPy loading can increase the ALP activity.

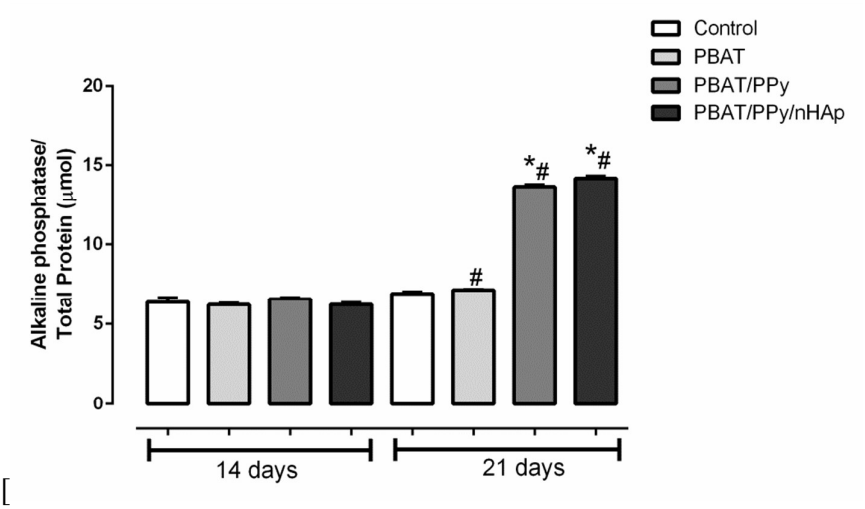

[

Figure 7. ALP activity after 14 and 21 days of osteoblasts culture with PBAT, PBAT/PPy and PBAT/PPy/nHAp scaffolds. *p<0.05 *vs* control group of the same period. #p<0.05 *vs* control group from 14 days.

The ability of PPy itself to induce osteoblastic differentiation had not been described yet and a possible explanation relies on wettability properties. **Fig. 8** shows snapshots taken at different times for PBAT and PBAT/PPy scaffolds. We observed an advanced contact angle (ACA, at 0 min) of 84º for PBAT/PPy, while for PBAT the ACA was quite higher (115º). Furthermore, the water drop was fully absorbed by PBAT/PPy scaffold after 7 min, while PBAT took 45 min, which is quite in agreement with recent studies. [20]

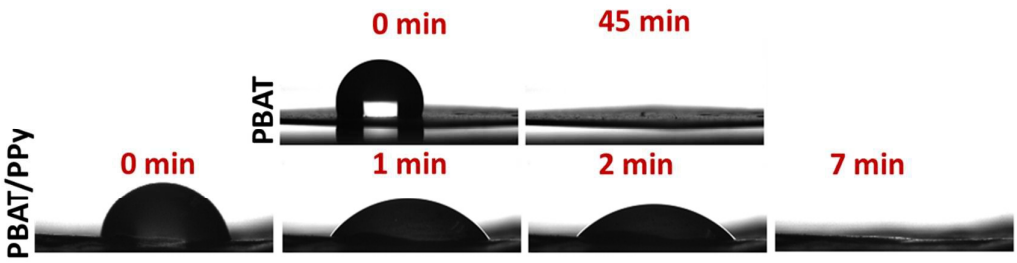

Figure 8. Snapshots taken at different times for PBAT and PBAT/PPy during contact angle measurements.

Some authors observed a relationship among surface hydrophobicity and cell spreading, osteodifferentiation and improvement of metabolic activity. [69-71] Therefore, changes in the hydrophilicity after PPy incorporation could be the responsible for the observed osteoblasts behavior and ALP activity.

4. Conclusions

Herein we present for the first time the production of conductive and hydrophilic PBAT/PPy mats using electrospinning technique. We electrodeposited stoichiometric nHAp crystals onto PBAT/PPy mats and produced a novel nanocomposite with potential of application in bone tissue engineering. The PBAT/PPy/nHAp nanocomposites presented biocompatibility, providing a good surface for cellular adhesion and the induction of osteoblasts differentiation. All these characteristics are very illustrative and could accelerate bone formation and implant fixation. Further investigations are required to verify the application of this novel nanobiomaterial and will be carried out in our lab.

Acknowledgments

The authors would like to thank National Council for Scientific and Technological Development (CNPq, 474090/2013-2), São Paulo Research Foundation (FAPESP, 2011/17877-7, 2011/20345-7), Brazilian Innovation Agency (FINEP) and Coordination for the Improvement of Higher Education Personnel (CAPES, 88887.095044/2015-00) for financial support. B. V. M. R. would also like to thank FAPESP for the postdoctoral fellowship (2015/08523-8).

5. References

1. H. Y. Mi, X. Jing and L. S. Turng, *Journal of Cellular Plastics*, 2014, **51**, 165-196.
2. D. W. Hutmacher, *Journal of Biomaterials Science, Polymer Edition*, 2001, **12**, 107-124.
3. G. C. Ingavle and J. K. Leach, *Tissue Engineering - Part B: Reviews*, 2014, **20**, 277-293.
4. S. Khorshidi, A. Solouk, H. Mirzadeh, S. Mazinani, J. M. Lagaron, S. Sharifi and S. Ramakrishna, *Journal of Tissue Engineering and Regenerative Medicine*, 2015, DOI: 10.1002/term.1978.
5. J. S. Choi, H. S. Kim and H. S. Yoo, *Drug Delivery and Translational Research*, 2015, **5**, 137-145.
6. S. Kaur, S. Sundarrajan, D. Rana, R. Sridhar, R. Gopal, T. Matsuura and S. Ramakrishna, *Journal of Materials Science*, 2014, **49**, 6143-6159.
7. L. Weng and J. Xie, *Current Pharmaceutical Design*, 2015, **21**, 1944-1959.
8. B. D. Ulery, L. S. Nair and C. T. Laurencin, *Journal of Polymer Science, Part B: Polymer Physics*, 2011, **49**, 832-864.
9. M. Shah Mohammadi, M. N. Bureau and S. N. Nazhat, in *Biomedical Foams for Tissue Engineering Applications*, 2014, DOI: 10.1533/9780857097033.2.313, pp. 313-334.
10. M. Okamoto and B. John, *Progress in Polymer Science*, 2013, **38**, 1487-1503.
11. B. V. M. Rodrigues, A. S. Silva, G. F. S. Melo, L. M. R. Vasconscellos, F. R. Marciano and A. O. Lobo, *Materials Science and Engineering C*, 2016, **59**, 782-791.
12. S. P. Pawar, A. Misra, S. Bose, K. Chatterjee and V. Mittal, *Colloid Polym Sci*, 2015, **293**, 2921-2930.
13. W. A. R. Neto, A. C. C. de Paula, T. M. M. Martins, A. M. Goes, L. Averous, G. Schlatter and R. E. S. Bretas, *Polymer Degradation and Stability*, 2015, **120**, 61-69.

14. L. C. Arruda, M. Magaton, R. E. S. Bretas and M. M. Ueki, *Polym Test*, 2015, **43**, 27-37.
15. A. M. Goes, S. Carvalho, R. L. Orefice, L. Averous, T. A. Custodio, J. G. Pimenta, M. D. Souza, M. C. Branciforti and R. E. S. Bretas, *Polimeros-Ciencia E Tecnologia*, 2012, **22**, 34-40.
16. S. W. Ko, R. K. Gupta, S. N. Bhattacharya and H. J. Choi, *Macromolecular Materials and Engineering*, 2010, **295**, 320-328.
17. C. S. Wu, *Carbon*, 2009, **47**, 3091-3098.
18. L. Jiang, M. P. Wolcott and J. Zhang, *Biomacromolecules*, 2006, **7**, 199-207.
19. W. A. Ribeiro Neto, A. C. C. De Paula, T. M. M. Martins, A. M. Goes, L. Averous, G. Schlatter and R. E. Suman Bretas, *Polymer Degradation and Stability*, 2015, **120**, 61-69.
20. B. V. M. Rodrigues, A. S. Silva, G. F. S. Melo, L. M. R. Vasconscellos, F. R. Marciano and A. O. Lobo, *Materials Science and Engineering: C*, 2016, **59**, 782-791.
21. J. Prasanna, T. Monisha, V. Ranjithabala, R. Gupta, E. Vijayakumar and D. Sangeetha, *Journal*, 2014, **894**, 360-363.
22. A. M. Goes, S. Carvalho, R. L. Oréfice, L. Avérous, T. A. Custódio, J. G. Pimenta, M. De B. Souza, M. C. Branciforti and R. E. S. Bretas, *Polimeros*, 2012, **22**, 34-40.
23. B. S. Spearman, A. J. Hodge, J. L. Porter, J. G. Hardy, Z. D. Davis, T. Xu, X. Zhang, C. E. Schmidt, M. C. Hamilton and E. A. Lipke, *Acta biomaterialia*, 2015, **28**, 109-120.
24. B. G. X. Zhang, A. F. Quigley, D. E. Myers, G. G. Wallace, R. M. I. Kapsa and P. F. M. Choong, *International Journal of Artificial Organs*, 2014, **37**, 277-291.
25. T. Sudwilai, J. J. Ng, C. Boonkrai, N. Israsena, S. Chuangchote and P. Supaphol, *Journal of Biomaterials Science, Polymer Edition*, 2014, **25**, 1240-1252.
26. R. Balint, N. J. Cassidy and S. H. Cartmell, *Acta biomaterialia*, 2014, **10**, 2341-2353.
27. L. Liu, P. Li, G. Zhou, M. Wang, X. Jia, M. Liu, X. Niu, W. Song, H. Liu and Y. Fan, *Journal of Biomedical Nanotechnology*, 2013, **9**, 1532-1539.
28. Y. Sharma, A. Tiwari and H. Kobayashi, in *Biomedical Materials and Diagnostic Devices*, 2012, DOI: 10.1002/9781118523025.ch19, pp. 581-593.
29. A. A. Marino and R. O. Becker, *Nature*, 1970, **228**, 473-&.
30. S. Baiotto and M. Zidi, *Biomechanics and Modeling in Mechanobiology*, 2004, **3**, 6-16.
31. J. Ferrier, S. M. Ross, J. Kanehisa and J. E. Aubin, *Journal of Cellular Physiology*, 1986, **129**, 283-288.
32. S. D. McCullen, J. P. McQuilling, R. M. Grossfeld, J. L. Lubischer, L. I. Clarke and E. G. Loboa, *Tissue Engineering - Part C: Methods*, 2010, **16**, 1377-1386.
33. K. Anselme, *Biomaterials*, 2000, **21**, 667-681.
34. B. Miara, E. Rohan, M. Zidi and B. Labat, *Journal of the Mechanics and Physics of Solids*, 2005, **53**, 2529-2556.
35. H. Zanin, C. M. R. Rosa, N. Eliaz, P. W. May, F. R. Marciano and A. O. Lobo, *Nanoscale*, 2015, **7**, 10218-10232.
36. M. A. V. M. Grinet, H. Zanin, A. E. Campos Granato, M. Porcionatto, F. R. Marciano and A. O. Lobo, *Journal of Materials Chemistry B*, 2014, **2**, 1196-1204.

37. I. A. W. B. Siqueira, M. A. F. Corat, B. D. N. Cavalcanti, W. A. R. Neto, A. A. Martin, R. E. S. Bretas, F. R. Marciano and A. O. Lobo, *ACS Applied Materials and Interfaces*, 2015, **7**, 9385-9398.
38. G. Wei and P. X. Ma, *Biomaterials*, 2004, **25**, 4749-4757.
39. H. Wang, Y. Li, Y. Zuo, J. Li, S. Ma and L. Cheng, *Biomaterials*, 2007, **28**, 3338-3348.
40. J. Venkatesan and S.-K. Kim, *Journal of Biomedical Nanotechnology*, 2014, **10**, 3124-3140.
41. M. A. V. M. Grinet, H. Zanin, A. E. C. Granata, M. Porcionatto, F. R. Marciano and A. O. Lobo, *Journal of Materials Chemistry B*, 2014, **2**, 1196-1204.
42. M. M. Pérez-Madrigal, L. J. Del Valle, E. Armelin, C. Michaux, G. Roussel, E. A. Perpète and C. Alemán, *ACS Applied Materials and Interfaces*, 2015, **7**, 1632-1643.
43. P. J. Molino, P. C. Innis, M. J. Higgins, R. M. I. Kapsa and G. G. Wallace, *Synthetic Metals*, 2015, **200**, 40-47.
44. A. Mihic, Z. Cui, J. Wu, G. Vlacic, Y. Miyagi, S. H. Li, S. Lu, H. W. Sung, R. D. Weisel and R. K. Li, *Circulation*, 2015, **132**, 772-784.
45. C. Ungureanu, S. Popescu, G. Purcel, V. Tofan, M. Popescu, A. Sălăgeanu and C. Pîrvu, *Materials Science and Engineering C*, 2014, **42**, 726-733.
46. J. Thunberg, T. Kalogeropoulos, V. Kuzmenko, D. Hägg, S. Johannesson, G. Westman and P. Gatenholm, *Cellulose*, 2015, **22**, 1459-1467.
47. A. S. Sarac, 2013.
48. E. Llorens, E. Armelin, M. D. M. Pérez-Madrigal, L. J. del Valle, C. Alemán and J. Puiggalí, *Polymers*, 2013, **5**, 1115-1157.
49. S. Cetiner, M. Olariu and A. S. Sarac, *Digest Journal of Nanomaterials and Biostructures*, 2013, **8**, 677-683.
50. T. Mosmann, *J Immunol Methods*, 1983, **65**, 55-63.
51. N. Eliaz and T. M. Sridhar, *Cryst Growth Des*, 2008, **8**, 3965-3977.
52. T. V. Vijayaraghavan and A. Bensalem, *J Mater Sci Lett*, 1994, **13**, 1782-1785.
53. N. Eliaz, W. Kopelovitch, L. Burstein, E. Kobayashi and T. Hanawa, *Journal of Biomedical Materials Research Part A*, 2009, **89A**, 270-280.
54. H. Fong, I. Chun and D. H. Reneker, *Polymer*, 1999, **40**, 4585-4592.
55. D. T. M. Thanh, P. T. Nam, N. T. Phuong, L. X. Que, N. V. Anh, T. Hoang and T. D. Lam, *Mat Sci Eng C-Mater*, 2013, **33**, 2037-2045.
56. K. Fukushima, A. Rasyida and M.-C. Yang, *Applied Clay Science*, 2013, **80–81**, 291-298.
57. M. B. Runge, M. Dadsetan, J. Baltrusaitis and M. J. Yaszemski, *Journal of biological regulators and homeostatic agents*, 2011, **25**, S15-S23.
58. J. Pelto, M. Björninen, A. Pälli, E. Talvitie, J. Hyttinen, B. Mannerström, R. Suuronen Seppanen, M. Kellomäki, S. Miettinen and S. Haimi, *Tissue Engineering. Part A*, 2013, **19**, 882-892.
59. A. Fahlgren, C. Bratengeier, A. Gelmi, C. M. Semeins, J. Klein-Nulend, E. W. H. Jager and A. D. Bakker, *PLoS ONE*, 2015, **10**, e0134023.
60. F. J. O'Brien, B. A. Harley, I. V. Yannas and L. J. Gibson, *Biomaterials*, 2005, **26**, 433-441.
61. S. J. Lee, J. S. Choi, K. S. Park, G. Khang, Y. M. Lee and H. B. Lee, *Biomaterials*, 2004, **25**, 4699-4707.
62. J.-P. Chen and Y.-S. Chang, *Colloids and Surfaces B: Biointerfaces*, 2011, **86**, 169-175.
63. Y. He, Y. Dong, F. Cui, X. Chen and R. Lin, *PLoS ONE*, 2015, **10**, e0135366.

64. R. Vasita and D. S. Katti, *International journal of nanomedicine*, 2006, **1**, 15-30.
65. E. M. Czekanska, M. J. Stoddart, J. R. Ralphs, R. G. Richards and J. S. Hayes, *Journal of Biomedical Materials Research Part A*, 2014, **102**, 2636-2643.
66. H. Orimo, *Journal of Nippon Medical School*, 2010, **77**, 4-12.
67. J. G. Hardy, M. K. Villancio-Wolter, R. C. Sukhavasi, D. J. Mouser, D. Aguilar, S. A. Geissler, D. L. Kaplan and C. E. Schmidt, *Macromolecular Rapid Communications*, 2015, **36**, 1884-1890.
68. H. Castano, E. A. O'Rear, P. S. McFetridge and V. I. Sikavitsas, *Macromolecular bioscience*, 2004, **4**, 785-794.
69. W. Jianhua, I. Toshio, O. Naoto, I. Takayasu, M. Takashi, L. Baolin and Y. Masao, *Biomedical Materials*, 2009, **4**, 045002.
70. D. Y. Eda, B. Robyn, P. Daphne, A. Fred, G. Selçuk and S. Wei, *Biofabrication*, 2010, **2**, 014109.
71. M. T. Khorasani, H. Mirzadeh and S. Irani, *Radiation Physics and Chemistry*, 2008, **77**, 280-287.

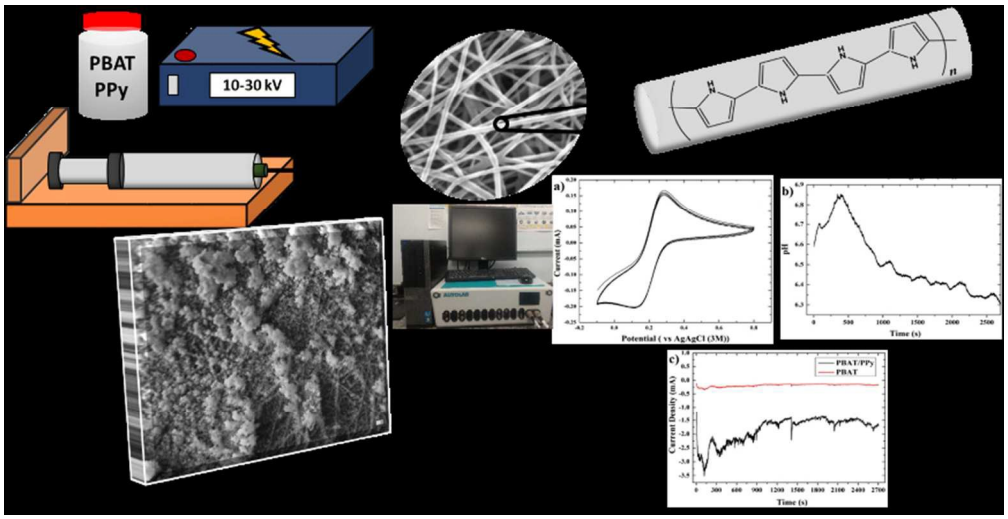

99x50mm (220 x 220 DPI)